The effect of annealing conditions on the physical properties of $Nd_{0.67}Sr_{0.33}MnO_{3-\delta}$

2000 J. Phys.: Condens. Matter 12 4401

(http://iopscience.iop.org/0953-8984/12/19/310)

J. Phys.: Condens. Matter **12** (2000) 4401–4416. Printed in the UK PII: S0953-8984(00)09151-7

The effect of annealing conditions on the physical properties of $Nd_{0.67}Sr_{0.33}MnO_{3-\delta}$

W Schnelle†, A Poddar‡, P Murugaraj§, E Gmelin, R K Kremer, K Sasaki‖ and J Maier

Max-Planck-Institut für Festkörperforschung, Heisenbergstraße 1, D-70569 Stuttgart, Germany

E-mail: schnelle@cpfs.mpg.de

Received 1 November 1999, in final form 9 March 2000

Abstract. A study of the influence of annealing in atmospheres with defined oxygen partial pressures (1.5×10^{-6} Pa $\leqslant P_{O_2} \leqslant 10^{+5}$ Pa) on the electrical resistivity $\rho(T)$, magnetic susceptibility $\chi(T)$, and heat capacity $c_p(T)$ of ceramic samples of $Nd_{0.67}Sr_{0.33}MnO_{3-\delta}$ is presented. $\rho(T)$ at 1000 °C shows no appreciable change for 10^{+2} Pa $\leqslant P_{O_2} \leqslant 10^{+5}$ Pa. For samples annealed in air a sharp peak is found in $c_p(T)$ and in $\rho(T)$ at the ferromagnetic transition ($T_C \approx 238$ K). The insulator–metal transition is observed below T_C as a broad peak in $\rho(T)$. Annealing at lower P_{O_2} leads to an increase of ρ whereas T_C decreases only by ≈2 K. Annealing at $P_{O_2} \leqslant 6.3 \times 10^{-2}$ Pa suppresses T_C and results in spin canting and a vanishing of the peak in $c_p(T)$. The specific heat (2–300 K) for samples annealed in air and in Ar/5% H_2 is determined and thermodynamic standard values are calculated. The problem of the separation of $c_p(T)$ into lattice, electronic, and Mn and Nd magnetic contributions is discussed. $c_p(T < 20$ K) is dominated by a Schottky-like anomaly from the Zeeman-split ground-state doublet of Nd^{3+}. A large quasi-linear term is mimicked by a broadening of the Schottky-like anomaly and by magnetic contributions from Mn in oxygen-deficient samples. The results are discussed in the context of oxygen deficiency δ, carrier concentration, defect chemistry, and disorder.

1. Introduction

The doped perovskite manganites $RE_{1-x}AE_xMnO_3$ (RE = La, Pr, Nd, Sm, etc; AE = Ca, Sr, Ba, etc) [1, 2] have attracted renewed interest [3–6] both as regards understanding the mechanism behind the 'colossal'-magnetoresistance (CMR) effect and for their applications to magnetoresistance (MR) sensors and electrochemical devices [7]. The end-members of this system are antiferromagnetic (afm) insulators [2, 4]. Partial substitution for the RE on the A site of the ABO_3 structure with a divalent alkaline-earth AE introduces mixed-valence Mn^{4+}/Mn^{3+} on the B site. With decreasing temperature the system undergoes a transition from the paramagnetic (pm) to the ferromagnetic (fm) state which traditionally has been explained by a magnetic coupling between the Mn^{4+} and Mn^{3+} via the double-exchange (DE) mechanism [8]. Around the temperature of the pm–fm transition, T_C, these systems also undergo an insulator–metal transition.

† Author to whom correspondence should be addressed. New address: Max-Planck-Institut für Chemische Physik fester Stoffe, Pirnaer Landstraße 176, D-01257 Dresden, Germany.
‡ New address: Saha Institute of Nuclear Physics, 1/AF Bidhannagar, Calcutta 700 064, India.
§ Permanent address: Indian Institute of Technology, Madras 600 036, India.
‖ New address: Kyushu-University, Kasuga-kouen, Kasuga-shi, Fukuoka 816-8580, Japan.

0953-8984/00/194401+16$30.00

The concentration n_h of Mn^{4+} holes controls the transport and magnetic properties [8–10]. For an optimized doping ($x \approx 1/3$ in $La_{1-x}Sr_xMnO_3$ or $Nd_{1-x}Sr_xMnO_3$), a large negative magnetoresistance is observed near T_C. For lower n_h the Mn spins cant and afm transitions are observed (for electronic phase diagrams see e.g. [5, 6, 11]). In addition, the manganites show structural transitions and a charge-ordered state, depending on n_h and on the bond-length mismatch [5, 6 11–13]. The transitions can also be driven by magnetic field [6,12] or pressure. Charge-ordered phases were reported for most $RE_{1-x}Sr_xMnO_3$ compounds [12–15]. Many aspects of the interplay between structure, charge, spin, and orbital degrees of freedom [4,5,11] are yet to be understood. For a proper explanation of the CMR one has to consider strong electron–phonon interactions arising from a Jahn–Teller distortion of MnO_6 octahedra, in addition to DE interactions [16].

Although the general behaviour of the resistivity and magnetization is similar for all the different samples of a specific $RE_{1-x}AE_xMnO_3$ composition studied, T_C, the peak resistivity, and the peak magnetoresistance appear to depend strongly on the sample preparation. One line of argumentation attributes the variations to grain boundaries, internal strains, or microcracks [17–21] while the other line holds variations in the bulk oxygen content δ responsible [21–24]. The formation of defects in $RE_{1-x}AE_xMnO_3$ is not fully clarified. Bulk oxygen defects are possible, and when the charge is compensated by a change of the Mn valence the composition can be written as

$$RE^{3+}_{1-x}AE^{2+}_{x}Mn^{3+}_{1-x+2\delta}Mn^{4+}_{x-2\delta}O^{2-}_{3-\delta}. \tag{1}$$

Since the degree x of AE-cation substitution along with the oxygen deficiency δ determines the Mn^{4+} content (and, hence, the hole concentration $n_h = x - 2\delta$), annealing in a different atmosphere, which alters δ via the oxygen exchange equilibrium, affects the transport and magnetic properties. For $\delta = x/2$, all Mn^{4+} are reduced to Mn^{3+}; that is, $n_h \approx 0$. Oxygen excess cannot be accommodated in interstitial positions of the dense-packed perovskite structure, and oxidation leads to cation vacancies [4, 25].

Ju *et al* [26, 27] studied the resistivity, magnetization, and MR of $La_{0.67}Ba_{0.33}MnO_{3-\delta}$ and $Nd_{0.67}Sr_{0.33}MnO_{3-\delta}$ polycrystalline samples. They observed that with increasing δ the resistivity increases and T_C shifts to lower T. Essentially the same behaviour was found for $La_{0.85}Sr_{0.15}MnO_{3-\delta}$ single crystals [24]. Resistivity measurements on fully oxygen-annealed samples [17, 18, 28] show a peak at a temperature, T_{max}, which coincides with T_C, whereas in the case of air-annealed samples T_{max} deviates from T_C (in most cases $T_{max} < T_C$). There is also a large variation of T_{max} and T_C and in the magnitude of the MR for samples of apparently similar composition.

The application of pressure P and the partial substitution with a RE of different radius, r_A, reveal a direct relationship between T_C and P/r_A [1,29]. These results establish that there is a significant coupling between charge carriers and phonons which is manifested also in a huge oxygen isotope effect [30]. In this context, heat capacity experiments, which yield information on the total entropy (contributions from structural, magnetic, and electronic effects), could provide deeper insight into the carrier–phonon coupling. Low-temperature $c_p(T)$ data on $La_{1-x}Sr_xMnO_3$ have been reported in [31, 32], and measurements up to 300 K on the La–Ca system in [14, 33]. For $x \approx 0.33$, large peaks at T_C were found. Recently, measurements on the Nd–Sr system were published by Gordon *et al* [34]. Besides other findings, they observed a quite large specific heat term linear in T, which they assigned to a magnetic interaction of the Nd and Mn sublattices. $c_p(T)$ results for charge-ordered compositions are reported in [15,35].

Along with thermogravimetric analysis (TGA), specific heat and magnetization are probing the bulk while the (magneto-) resistivity depends strongly on the grain structure and lattice strain in the individual sample. A combination of these measurements can thus

discriminate between bulk and intergranular effects in polycrystalline samples.

In this paper, we report on the influence of annealing in atmospheres with controlled oxygen partial pressures on the properties of $Nd_{0.67}Sr_{0.33}MnO_{3-\delta}$. Although the detailed defect chemical situation in the 'frozen-in state' is expected to be complicated [7, 36], even for infinitely fast quenching, such a study can reveal important correlations between relevant magnetic and electronic properties and non-stoichiometry. According to the electronic phase diagram [5, 11], the Nd–Sr system with $x = 1/3$ displays a clear transition from a pm insulator to a fm metal. In Nd–Sr manganite there exist two magnetic sublattices. It is thought that at low T the Nd magnetism is influenced by the molecular field of the ordered Mn sublattice. This interesting situation occurs also for other oxides, e.g. $Nd_{1-x}Ce_xCuO_4$ [37] and $PrBa_2Cu_3O_{7-\delta}$ [38]. In the following we present the results of electrical resistivity (4 K–300 K), electrical conductivity (300 K–1273 K), magnetic susceptibility (4 K–300 K), and heat capacity measurements. For two samples subjected to different annealing procedures (producing strongly different values of δ), precise values of the specific heat were determined in the range 2 K–300 K.

2. Sample preparation and characterization

The samples were prepared by solid-state reaction using 3N-purity starting materials. Stoichiometric portions of Nd_2O_3, $SrCO_3$, and MnO_2 were mixed under ethanol using a Fritsch planetary ball mill equipped with a zirconia jar for 2 h. The slurry was dried and then calcined in an alumina crucible at 1200 °C for 24 h. This procedure was repeated three times with intermediate grinding (Retsch Vibromill). The resulting powder was pressed to a pellet and sintered at 1500 °C for 5 h in air, slowly cooled (30 °C h^{-1}) to 1300 °C, annealed there for 15 h, and finally cooled to room temperature (120 °C h^{-1}).

We prepared two series of samples from the same initial batch (see table 1). Series A consists of five samples: sample A2 is the pristine material, while A1, A3, A4, and A5 were subjected to additional annealing. The rate of cooling to room temperature was 120 °C h^{-1}. For series B (samples B1–B7) we restricted the annealing to a constant T_{ann} of 1000 °C, except

Table 1. Temperatures, times, atmospheres, oxygen partial pressures of the atmospheres for the annealing, and pseudo-cubic lattice parameters a (error ±0.03 pm, typically) for the ceramic $Nd_{0.67}Sr_{0.33}MnO_{3-\delta}$ samples.

Sample	T_{ann} (°C)	t_{ann} (h)	Atmosphere	P_{O_2} (Pa)	a (pm)
A1	1300	+ 15	O_2	$1.0 \times 10^{+5}$	384.5
A2	1300	n/a	Air	$2.1 \times 10^{+4}$	385.2
A3	1000	+ 10	Ar	$\approx 10^{+1}$	386.0
A4	1100	+ 15	Ar	$\approx 10^{+1}$	386.0
A5	400	+ 5	Ar/5% H_2	($<10^{-15}$)	—
B1	1000	+ 40	O_2	$1.0 \times 10^{+5}$	385.6
B2	1000	n/a	Air	$2.1 \times 10^{+4}$	385.6
B3	1000	+ 40	Ar/O_2	$1.0 \times 10^{+3}$	385.6
B4	1000	+ 40	Ar/O_2	$1.0 \times 10^{+1}$	385.7
B5	1000	+ 40	Ar/H_2/H_2O	6.3×10^{-2}	385.5
B6	600	+ 5	Ar/5% H_2	($<10^{-15}$)	386.3
B7	1000	+ 40	Ar/H_2/H_2O	1.5×10^{-6}	—
X2	1250	n/a	Air	$2.1 \times 10^{+4}$	—

for sample B6. The samples were heated for 40 h in atmospheres with carefully controlled oxygen partial pressures. For P_{O_2} ranging from 10^{+5} Pa to 10^{+1} Pa, Ar–O_2 mixtures with known P_{O_2} were used. For more reducing conditions down to 1.5×10^{-6} Pa, Ar–H_2–H_2O mixtures were used, in which P_{O_2} is fixed by H_2 and H_2O partial pressures and was checked by a zirconia-based sensor. Sample B6 was annealed in 95% Ar/5% H_2 at 600 °C. P_{O_2} for such an atmosphere is $<10^{-15}$ Pa, but we expect the reduction kinetics at 600 °C to be sluggish and 5 h annealing too short, so the effective P_{O_2} for sample B6 may be between those of B5 and B7, as confirmed by the $\rho(T)$ data.

X-ray powder diffractograms taken before sintering and after annealing indicate single-phase materials with a distorted, nearly cubic structure (pseudo-cubic lattice parameter; see table 1). Only sample B7 showed additional phases, i.e. annealing under $P_{O_2} = 1.5 \times 10^{-6}$ leads to decomposition of the perovskite. For an additional sample (X2) from an earlier batch of the same composition, the specific heat was measured. $c_p(T)$ reveals Mn_3O_4 impurities which could not be detected by means of x-rays. Samples A1–A5 were chemically analysed by the ICP method. They consistently have the cationic composition $Nd_{0.67}Sr_{0.33}Mn_{1.00}$. Density measurements for the sintered pellets gave 6.37 g cm^{-3} (x-ray density 6.56–6.67 g cm^{-3}). To get an impression of the magnitude of the change of δ, one piece of as-prepared material was measured by TGA. In argon ($P_{O_2} \approx 10^{+1}$ Pa) at 1000 °C, a weight loss of 58.34 μg g^{-1} was found after 5 h, corresponding to a change of δ by 0.008 75. The absolute oxygen deficiency, δ, however, is unknown.

3. Experimental details

For the high-T conductivity measurements, pieces of as-prepared material were mounted in a cell made of quartz glass which is fitted with four Pt foil electrodes spot welded to Pt wires. Gas mixtures with well defined partial pressures are purged into the cell at room temperature for 5 h. Then the cell is heated to 1000 °C and annealed for 1 h. The voltages across the samples are monitored with a 5 mA current in the cooling cycle.

The low-T resistivity measurements were performed with a standard dc four-probe technique with silver epoxy contacts. Magnetization measurements were carried out with a SQUID magnetometer (MPMS, Quantum Design) in a field of 0.01 T.

The heat capacities of the samples A2 and B6 were measured using a quasi-adiabatic step-heating method [39] (Nernst's method). The heat capacity of the addenda was determined in a separate run and subtracted from the raw data. The inaccuracy of $c_p(T)$ is $\approx$1%. Additional determinations of $c_p(T)$ from 110–300 K for all samples were performed with a power-compensated differential scanning calorimeter (DSC; Perkin–Elmer DSC-2).

4. Results and discussion

4.1. High-temperature electrical conductivity

The high-T conductivity (figure 1) for all values of P_{O_2} investigated increases with T and saturates above 750 K, and is then essentially constant up to 1000 °C. The activation energy for the conduction is $\approx$0.13 eV, so the conductivity change in this temperature range spans only one order of magnitude. There is no significant change in electronic conductivity for the samples annealed at pressures in the P_{O_2}-range studied (10^{+5}Pa $\geqslant P_{O_2} \geqslant 10^{+2}$ Pa).

The substitution of hypovalent Sr^{2+} in the Nd^{3+} sublattice (Sr'_{Nd}) can be compensated either by positively charged electron holes (localized at Mn^{3+}, i.e. $Mn^{\bullet}_{Mn}$) or by positively charged

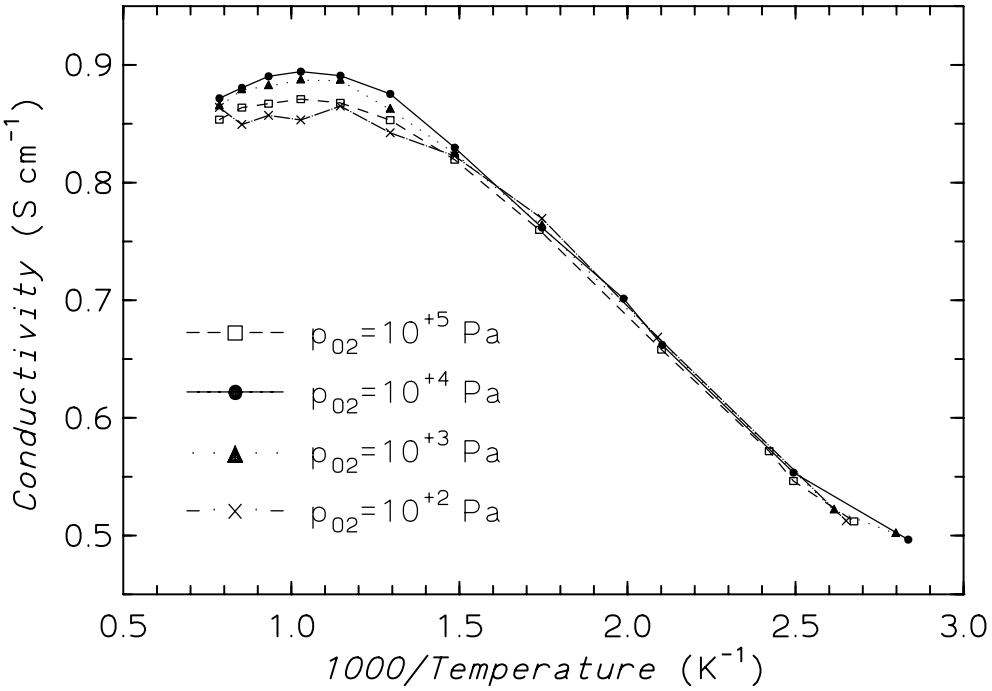

Figure 1. High-temperature electrical conductivity versus inverse temperature for a sample of $Nd_{0.67}Sr_{0.33}MnO_{3-\delta}$ in atmospheres of different oxygen partial pressures P_{O_2}.

oxygen vacancies ($V_o^{\bullet\bullet}$), as the electroneutrality condition

$$[Sr'_{Nd}] = 2[V_o^{\bullet\bullet}] + [Mn^{\bullet}_{Mn}]$$

holds, described using the Kröger–Vink notation [40]. Together with the small weight loss in the TGA, the high-T conductivity indicates that in $Nd_{0.67}Sr_{.33}MnO_{3-\delta}$ perovskite, Sr^{2+} substitution is predominantly charge compensated by valence changes in the Mn sublattice rather than generating oxygen vacancies, i.e. formula (1) is valid and n_h can be changed by varying δ.

4.2. Low-temperature electrical resistivity

The right-hand panel of figure 2 shows $\rho(T)$ for samples A1–A4. The curves are identical for heating and cooling cycles. In contrast to the case for the high-T data, drastic changes with variation of the annealing atmosphere are visible. $\rho(T)$ generally increases as P_{O_2} decreases. Samples A1 and A2 display two distinct features. On decreasing T from 300 K, $\rho(T)$ increases, peaks around 246 K, and then strongly decreases around 225 K. At still lower T, a shoulder-like feature appears. The curves are considered to arise from a superposition of two contributions: one being connected with the fm ordering at $T_C \approx 246$ K and the other signalling a transition $\approx$40 K below. Sample A3 shows higher ρ and now the lower temperature anomaly is dominant, and the apparent insulator–metal transition, if assigned at the temperature of the resistivity maximum, T_{max}, is shifted drastically to lower T. For sample A4 the prominent feature is the broad anomaly centred around 200 K. The signature of the pm–fm transition is submerged under this anomaly.

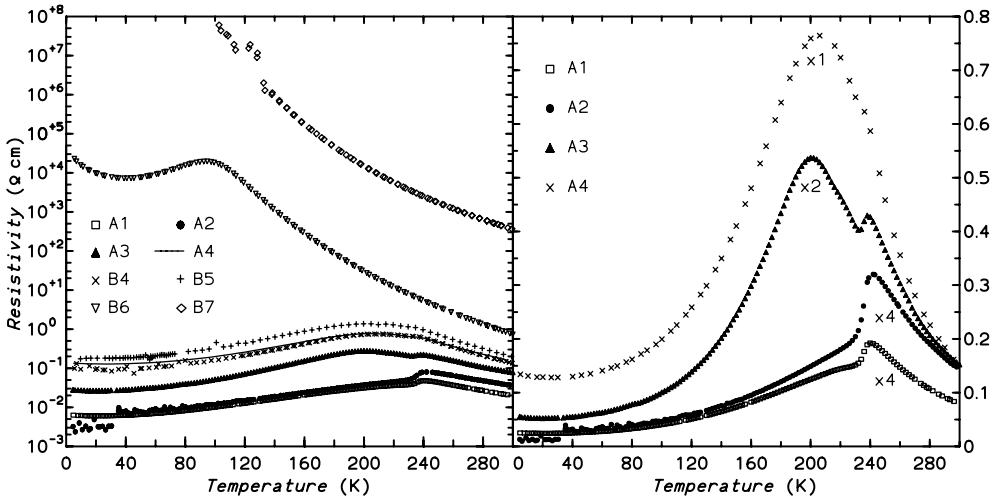

Figure 2. Electrical resistivity $\rho(T)$ for $Nd_{0.67}Sr_{0.33}MnO_{3-\delta}$ samples annealed under different conditions (see table 1). *Left:* $\rho(T)$ for samples A1–A4 and B4–B7 plotted on a logarithmic scale. *Right:* samples A1–A4. In order to resolve finer details, the data for samples A1 and A2 were multiplied by 4, and those of sample A3 by 2.

The $\rho(T)$ for samples from both series are displayed in the left-hand panel of figure 2. In general, a continuation of the trend towards higher ρ is observed. Sample B4 shows essentially the same curve as sample A4. Annealing under $P_{O_2} < 10^{-2}$ Pa changes the behaviour. $\rho(T)$ for sample B6 increases strongly with decreasing T down to $\approx$100 K, then shows a broad maximum and then decreases to $\approx$40% of the maximum value. Below 40 K, $\rho(T)$ again increases. This is similar to the behaviour of $La_{0.67}Ba_{0.33}MnO_{2.80}$ [26]. $\rho(T)$ for sample B7 is two orders of magnitude higher and shows no peak indicative of a insulator–metal transition before the maximum resistance measurable with our apparatus is reached. Together with the phase analyses of the latter two samples, this behaviour suggests that sample B6, even though annealed at a nominally extremely low P_{O_2}, had not been fully reduced due to the low annealing temperature and too-short duration.

Also, for other manganites, two separate anomalies in $\rho(T)$ were observed [26, 41]. For most bulk samples, T_{max} is different from T_C [2]. This result was attributed to an inhomogeneous distribution of the substituted cations or of oxygen vacancies. The presence of microscopic regions with slightly varying distribution of substituted cations may lead to a wide range of T_C. Such micro-inhomogeneities are well known in many complex oxides. The fact that in our samples with (presumably) small δ the pm–fm transitions in $\rho(T)$ are sharp and occur at the same T_C can be taken as evidence for a homogeneous distribution of the Sr cations and of the oxygen defects, as confirmed by our $c_p(T)$ data. Intergranular effects are another issue of importance. The general increase of ρ with δ might be partially caused by the degradation of grain boundaries.

4.3. Magnetic susceptibility

Susceptibility ($B_{ext} = 0.01$ T) curves $\chi(T)$ in the field-cooled (fc) and zero-field-cooled modes (zfc) are plotted in figure 3. Samples A1–A4 and B5 display a sharp pm–fm transition at 246 K (width <5 K) attributed to the fm spin ordering in the Mn sublattice. T_C, as determined from the inflection point of $\chi(T)$, is the same as that deduced from the sharp peak in $\rho(T)$. χ_{fc} increases

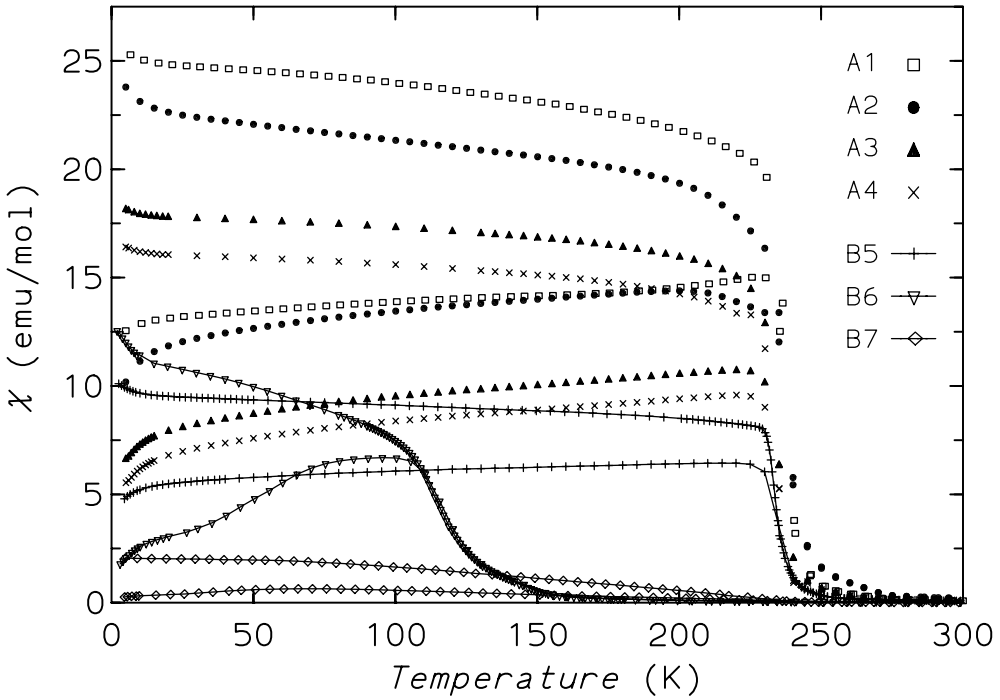

Figure 3. Magnetic susceptibility in an external field of 0.01 T in zero-field-cooled (zfc; lower branches) and field-cooled (fc; upper branches) modes, respectively.

only slowly below T_C, typical for a ferromagnet with domain motion. The small upturn ($\Delta\chi$) below 25 K in χ_{fc} is mirrored in the smaller χ_{zfc} by a downturn. This feature is absent for the La–Ca system [27] but present for other Nd–Sr samples [27], and is obviously associated with Nd magnetism. However, a $\Delta\chi$ of 1–2 emu mol^{-1} is too large to be accounted for by the paramagnetic signal of 0.67 Nd^{3+} mol^{-1} alone. Samples B1–B4 behave essentially identically to samples A1–A4 as regards $\chi(T)$. Samples B6 and B7 show a significantly reduced $\chi(T)$. While sample B5 still displays fc and zfc curves similar to those of samples A1–A4, sample B7 shows no clear magnetic transition but a smooth increase of the fc magnetic moment with decreasing T which starts near the value of T_C for samples A1–A4 and B5. We attribute this behaviour to the remaining ferromagnetic phase in this nearly decomposed sample. Sample B6 displays a broad magnetic phase transition near 120 K with a very pronounced difference between χ_{fc} and χ_{zfc}. Sample B6 also shows the upturns and downturns in χ_{fc} and χ_{zfc} below 25 K, while they are not observed for sample B7.

Isothermal dc magnetization loops for sample A2 taken at 220 K, 50 K, and 5 K display only small hystereses (e.g. at 5 K: $B_{coer} \approx 12$ mT, $M_{rem} \approx 0.21\ \mu_B$). The magnetization at 1 T is 3.72 μ_B which is about the spin-only value of the Mn^{4+}/Mn^{3+} mixture (3.67 μ_B). The loops for sample B6 at 120 K, 50 K, and 5 K are more pronounced (at 5 K: $B_{coer} \approx 60$ mT, $M_{rem} \approx 0.06\ \mu_B$). The magnetization at 1 T is only 0.33 μ_B and still irreversible. B_{coer} and M_{rem} for the loops of both samples at the highest temperatures are only ≈1/4 of the corresponding values at 5 K. Also, the spontaneous magnetic moment decreases systematically with decreasing P_{O_2} of the annealing atmosphere (i.e. increasing δ). For sample B6 these findings indicate a canting of the Mn spins as observed for cation-doped samples with $x < 0.33$. The large splitting between χ_{fc} and χ_{zfc} and the maximum in χ_{zfc} for sample B6 can be

interpreted as spin freezing, like that for a spin glass.

Worledge *et al* [42] observed that in $La_{0.67}Ca_{0.33}MnO_3$ films T_C increases with increasing annealing temperature, T_{ann}, and annealing time in Ar all the way from 78 K up to 274 K. Further increase in T_{ann} as well as annealing in O_2 did not appreciably change T_C. The authors explain the shift by the release of strain in the Mn–O–Mn bonds with increasing T_{ann}. Itoh *et al* [43] found an increase of T_C with increasing pressure and duration of oxygen annealing which, according to the authors, results from the relaxation of the lattice distortion and enhances the DE interaction.

In contrast to these results, the annealings of our Nd–Sr samples at the 100 K lower temperature T_{ann}, which significantly alter $\rho(T)$ and $\chi(T)$, do not produce any pronounced shift of T_C. This indicates that the samples are already well annealed at 1300 °C with a homogeneous distribution of cations. However, we noticed that when a sample was not sufficiently annealed, it always shows a pm–fm transition width >25 K and the insulator–metal transition occurs at much lower T. Also one may consider different residual P_{O_2} of the Ar. We conclude that for a defined sample preparation, a strict control of P_{O_2} and T_{ann} is necessary. In that respect, the relatively slow cooling rate of our samples is not problematic, since the oxygen diffusion in acceptor-doped manganites is known to be very sluggish [7, 36]. However, P_{O_2} can also be defined by other means. Ju *et al* [27, 28] used a Ti getter and found that their oxygen-deficient samples were magnetically inhomogeneous. δ for their samples is presumably in the same range as for our samples B5–B7, since significant changes in T_C and $\chi(T)$ were observed. The slight increase of the pseudo-cubic lattice parameter a for series A with increasing δ is expected, since Mn^{3+} is larger than Mn^{4+} (CN = 6), as already noted for $La_{0.67}Ba_{0.33}MnO_{3-\delta}$ [26]. However, there is no clear tendency in a for our series B.

4.4. Specific heat capacity

In figure 4 specific heat data obtained by DSC in the vicinity of the pm–fm transition are presented. Samples A1–A4 (not shown) display well defined peaks at 235–238 K, in agreement with T_C identified in $\chi(T)$. The values of T_C for samples A3 and A4 are slightly lower than those for samples A1 or A2. In series B (figure 4), the three samples annealed with 10^{+5} Pa $\geqslant P_{O_2} \geqslant 10^{+3}$ Pa display essentially identical peak shape and have the same T_C. Samples annealed under $P_{O_2} = 10^{+1}$ Pa and 6.3×10^{-2} Pa have slightly lower values of T_C, in agreement with $\chi(T)$. For sample B5 the peak height is decreased. Finally, for samples B6 and B7 there is no peak in the range of the DSC and $c_p(T)$ is drastically reduced.

Figure 5 shows $c_p(T)/T$ versus T for samples A2 and B6 in the range 1.5 K to 300 K. For sample A2 (as prepared), two anomalies appear: the magnetic phase transition at $T_C = 246$ K and a broad Schottky-like anomaly around 5 K. The peak maximum found by the fast DSC method occurs at a lower T_C in the slow heat pulse method. This 'delay' is one of the properties characteristic of a first-order transition which displays a time lag due to a coupling to the lattice. Structural distortions at T_C are demonstrated for several manganites [12, 20, 35]. $c_p(T)$ for sample B6 (Ar/5% H_2 annealed) is drastically different. No trace of a peak at T_C nor of the Schottky-like anomaly can be found. There is, however, an enormous excess specific heat between 7 K and ≈160 K and a reduced $c_p(T)$ above 160 K. A broadened jump-like anomaly at ≈120 K can be seen. For both samples we find no further anomalies, especially not for ≈43 K, where the strong magnetic ordering peak of Mn_3O_4 was found for the $x = 0.33$ sample in [34].

The thermodynamic standard values for enthalpy and entropy at 298.15 K are calculated by integration of $c_p(T)$. Below the lowest measured temperature, a T^3-extrapolation for $c_p(T)$ was employed. For sample A2 we find (including the transition) $\Delta_0^{298.15\ K} H^\circ =$

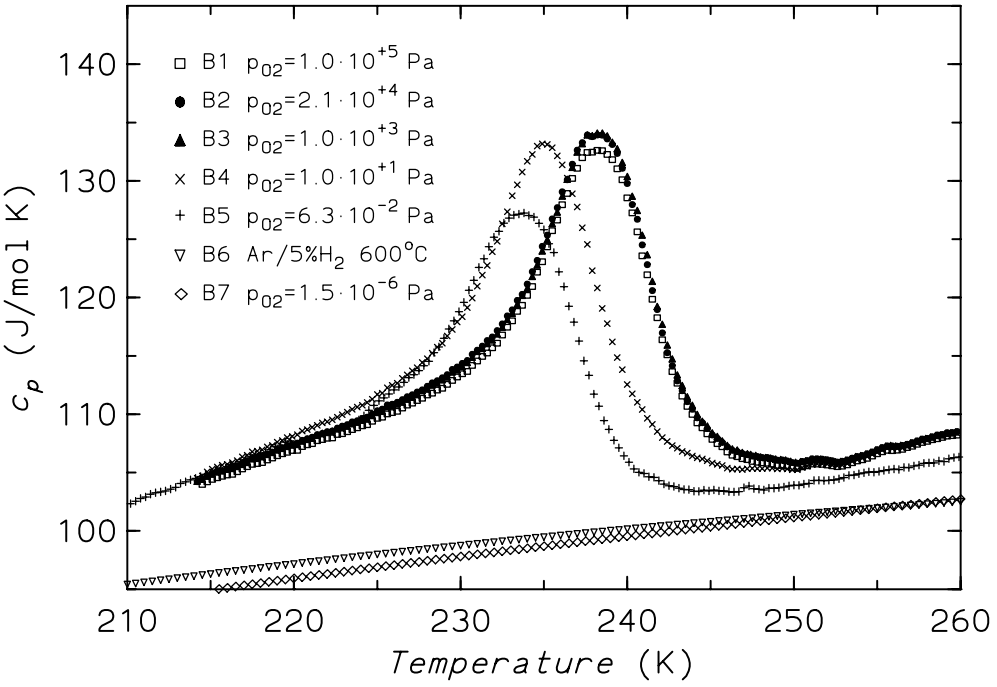

Figure 4. Temperature dependence of the specific heat $c_p(T)$ near the magnetic phase transition of $Nd_{1-x}Sr_xMnO_{3-\delta}$ as measured by DSC for the samples of series B.

20.88 ± 0.25 kJ mol^{-1} and $\Delta_0^{298.15\ \mathrm{K}}S^\circ = 132.5 \pm 1.6$ J mol^{-1} K^{-1}. For sample B6 we calculate $\Delta_0^{298.15\ \mathrm{K}}H^\circ = 20.66 \pm 0.25$ kJ mol^{-1}, which is the same value as for sample A2. However, we obtain a larger $\Delta_0^{298.15\ \mathrm{K}}S^\circ = 141.0 \pm 1.6$ J mol^{-1} K^{-1} ($\approx$1.0 R more than for sample A2). This difference is due to the excess specific heat of this sample below 160 K with respect to sample A2 (figure 5, inset). A part of this excess specific heat might be due to a softening of the lattice with δ—an effect often encountered in oxides, e.g. in $YBa_2Cu_3O_{7-\delta}$. However, most of this excess entropy has to be of magnetic origin.

In order to calculate the specific heat contribution $\Delta c_{\mathrm{trs}} = c_p(T) - c_l(T)$ and the entropy $\Delta S_{\mathrm{trs}} = \int (\Delta c_{\mathrm{trs}}/T)\,\mathrm{d}T$ related to the Mn-sublattice pm–fm transition, we have to estimate the lattice contribution $c_l(T)$. To reconstruct $c_l(T)$, the measured $c_p(T)$ are converted into equivalent Debye temperatures $\Theta_D(T)$ using $c_p(T) = ND(\Theta_D(T)/T)$. $\Theta_D(T)$ displays a maximum near 150 K and then decreases strongly towards T_C. $c_l(T)$ is calculated from a smooth interpolation of $\Theta_D(T)$ in the range 150 K ($\Theta_D = 490$ K) to 270 K ($\Theta_D = 380$ K). Below 150 K and above 270 K we may set $\Delta c_{\mathrm{trs}} = 0$. In this way, we calculate $\Delta S_{\mathrm{trs}} = 2.7$ J mol^{-1} K^{-1}, which is only 20% of the entropy expected for the fm ordering of Mn^{4+}/Mn^{3+} ($0.33R \ln 4 + 0.67R \ln 5 = 1.54\ R$). Equally low values of ΔS_{trs} have been observed for $La_{0.8}Ca_{0.2}MnO_3$ [44], for $La_{0.67}Ca_{0.33}MnO_3$ [14], and for a Nd–Sr ceramic specimen of the same cationic composition as our samples [34]. It can be argued that the magnetic entropy is partially compensated by structural and/or electronic contributions involved in the transition. Strong magneto-elastic coupling often leads to reduced ΔS_{trs} [4,45], but a reduction to only 20% seems unreasonably large.

Disregarding the influence of oxygen defects and concomitant reductions of Θ_D, we may also take $c_p(T)$ for sample B6 for $T > 200$ K as an indication of $c_l(T)$ for sample A2.

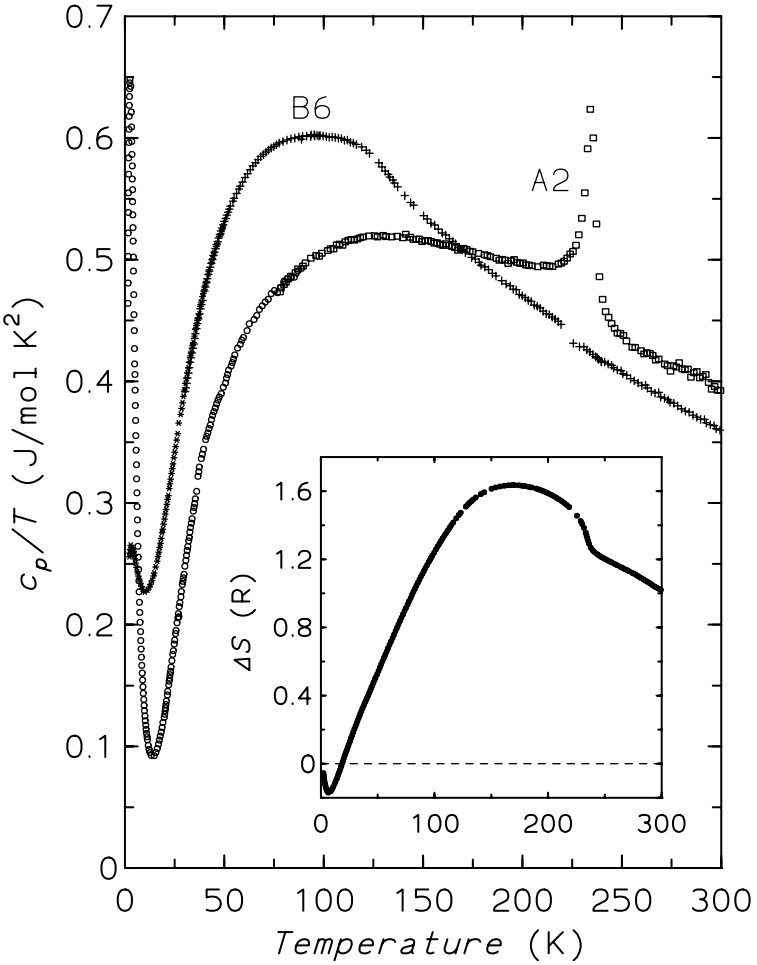

Figure 5. Specific heat for $Nd_{0.67}Sr_{0.33}MnO_{3-\delta}$ samples A2 and B6 as measured by the heat pulse method in a c_p/T versus T representation. *Inset:* the difference in entropy $\Delta S = S(T)[\mathrm{B6}] - S(T)[\mathrm{A2}]$ for the two samples.

The excess Δc_p for sample A2 with respect to sample B6 for $T > T_C[\mathrm{A2}]$ suggests that in the previous estimate a large amount of entropy from short-range correlations above T_C is missing. Since also in sample B6 the Mn sublattice orders at low T, it does not represent a 'non-magnetic' reference sample. Some Nd-related entropy (a Schottky anomaly of the Nd $J = 9/2$ multiplet) may contribute to ΔS. Nevertheless, the maximum ΔS between samples A2 and B6 (figure 5 inset) is $\approx$1.6 J mol^{-1} K^{-1}, i.e. of the expected size.

Figure 6 shows $c_p(T)$ for sample A2 around T_C in magnetic fields of 0, 2, and 7 T. With increasing field the peak at T_C gradually broadens and shifts to higher T while the entropy under the peak remains constant. The shift to higher T demonstrates the fm coupling of the Mn ions, while the conservation of the entropy under the peak shows that the associated structural distortions and the electronic transition move along with the magnetic transition to higher T. The height of the peak decreases with field and the peak temperature shifts proportionally to B_{ext} with $\Delta T_C/B_{\mathrm{ext}} \approx 5.5$ K T^{-1}. Park *et al* [46] measured $c_p(T)$ for $La_{0.7}Ca_{0.3}MnO_3$ for $B_{\mathrm{ext}} = 0.5$ T and 1 T. They found $\Delta T_C/B_{\mathrm{ext}} \approx 9$ K T^{-1} for both $c_p(T)$ and $\rho(T)$ but,

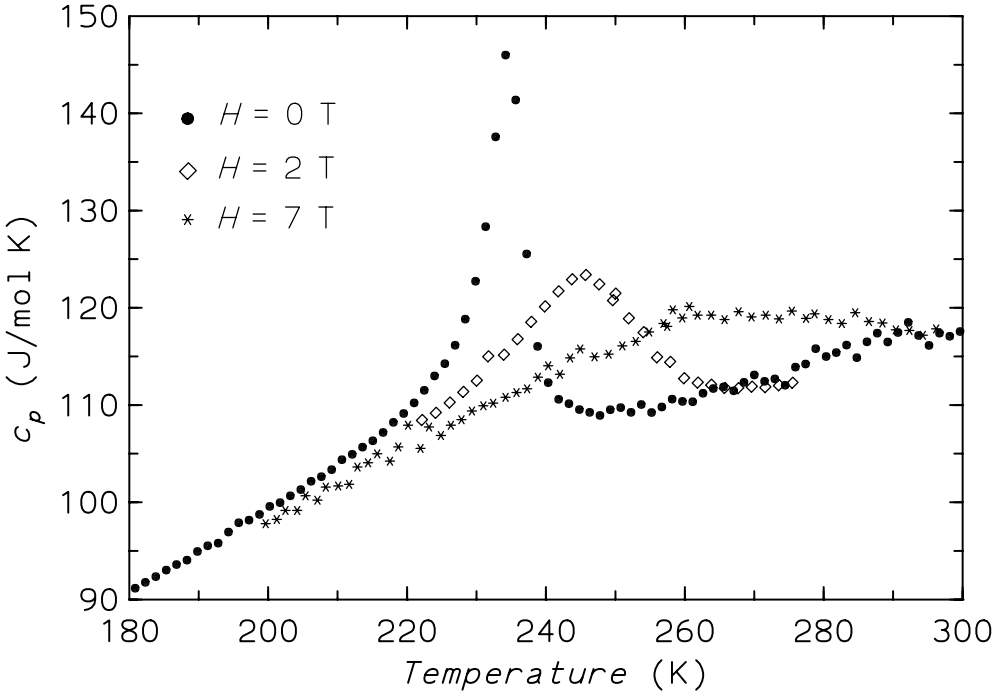

Figure 6. Magnetic field dependence of the specific heat of sample A2 near T_C.

in contrast, a non-monotonic decrease of the c_p-peak height with field. The application of pressure on Nd–Sr samples with $x = 0.33$ leads to a similar broadening and shift of the maximum in $\rho(T)$ to higher T [29].

4.5. Low-temperature specific heat

In figures 7 and 8 the low-T heat capacities of samples A2, B6, and X2 are displayed. For both sample A2 and X2 we find a Schottky-like anomaly in $c_p(T)$ below 14 K. Sample B6 shows no anomaly but has a large excess heat capacity for $T > 7$ K in comparison to sample A2. There is also a small excess heat capacity for sample X2 with respect to A2 for $T > 5$ K. For this sample the Schottky-like anomaly is broader and smaller than for sample A2. At 42.5 K an anomaly is found for sample X2 which can be related to the magnetic ordering of a Mn_3O_4 impurity. From the peak height for the Nd–Sr sample of Gordon *et al* [34], which is reported to contain 1.5 mol% of Mn_3O_4, we calculate <0.3 mol% Mn_3O_4 for our sample X2. Samples A2 and B6 show no Mn_3O_4 peak. Magnetic order of the Nd sublattice was not found in our samples for $T > 2$ K.

The $J = 9/2$ ground multiplet of Nd^{3+} is split into five Kramers doublets by the crystalline electric field. For Nd^{3+} in (Nd, Sr)$MnO_{3-\delta}$ we expect an energy splitting of >100 K between the ground doublet and the first excited doublet, since in the structurally related perovskite $NdGaO_3$ [47] and also in $NdBa_2Cu_3O_7$ [48] this level is situated at 132 K and 139 K, respectively. Therefore, in $Nd_{0.67}Sr_{0.33}MnO_{3-\delta}$, just the ground doublet accounts for the Schottky-like anomaly. This Kramers doublet is split by the molecular field of the ordered Mn sublattice. The entropy contained in the anomaly is $0.67R \ln 2$, as required. The anomaly in $c_p(T)$ is obviously related to the upturns and downturns in χ_{fc} and χ_{zfc} in the same temperature

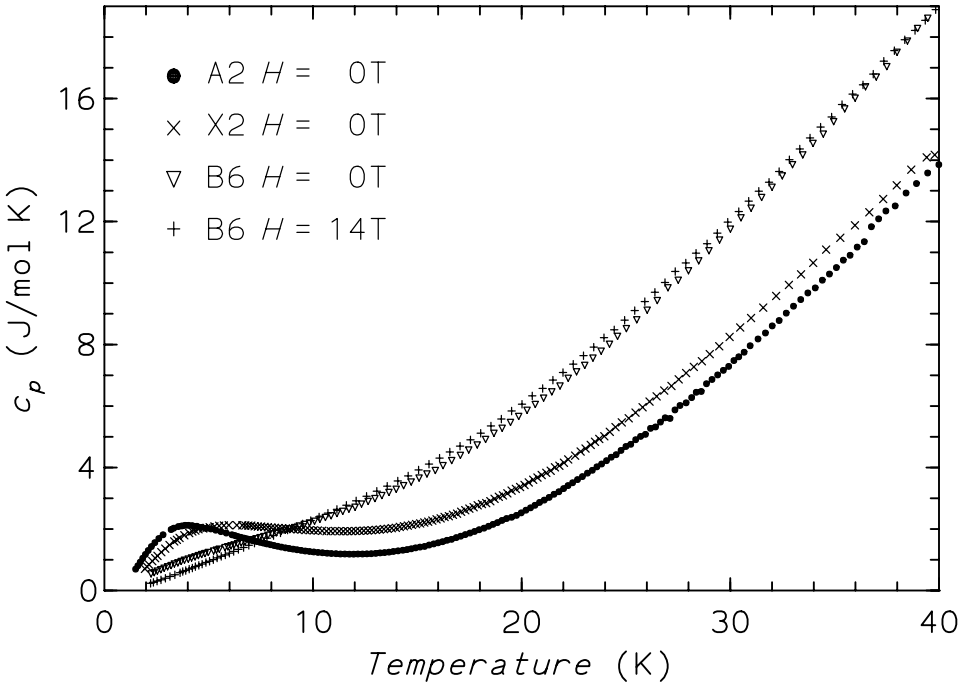

Figure 7. Specific heat capacities $c_p(T, B_{\mathrm{ext}})$ of samples A2 and X2 (0 T) and of sample B6 (0 T and 14 T external magnetic fields).

range. The size of this feature demonstrates the remarkable strength of the interaction between the two magnetic sublattices.

The energy splitting, ΔE, can be determined by a fit to $c_p(T)$. The data cannot be fitted by a simple two-level Schottky term. We could fit the data for sample A2 by adding up the contributions of three Schottky curves with values of $\Delta E = 5.8$ K, 9.7 K, and 12.9 K with a sum weight of 1/3 each (see figure 8). This is equivalent to a Gaussian broadening of the excited level. For the background specific heat we used a lattice term with $\Theta_{\mathrm{D}} = 340$ K. The fit is relatively insensitive to the addition of a linear γT-term of some mJ mol^{-1} K^{-2}; thus we have chosen $\gamma = 0$. For $La_{0.67}Sr_{0.33}MnO_3$, electronic γ-values of 6 mJ mol^{-1} K^{-2} ($\Theta_{\mathrm{D}} = 353$ K) [31] and 3.3 mJ mol^{-1} K^{-2} ($\Theta_{\mathrm{D}} = 289$ K) [32] have been observed. The broad distribution of ΔE originates from the statistical distribution of the Mn^{4+} and Mn^{3+} ions on the B sites in the Nd–Sr samples, giving rise to statistical internal exchange fields which are probed via the Zeeman splitting of the Nd-ion ground state. Similar effects have been observed in, e.g., rare-earth pyrochlores [49].

Sample X2 displays a smaller and broader Schottky-like anomaly. $c_p(T)$ can be modelled by a slightly 'softer' lattice term with $\Theta_{\mathrm{D}} = 325$ K and the sum of three Schottky anomalies at 7.5 K, 13.5 K, and 20.0 K (each of weight 1/3). Thus, the energy distribution of the splitting is wider for sample X2 than for A2. The agreement of the model with the data is poor (see figure 8) because there is significantly more entropy than is available from the Nd^{3+} Schottky excitation. The magnetic contribution of the minor Mn_3O_4 impurity is too much less to count, so the excess entropy has to stem from the Mn sublattice of the main phase. The small excess Δc_p increases with T and can be approximately described by a term $\gamma^* T$ or by $dT^{3/2}$ as for a fm spin-wave contribution.

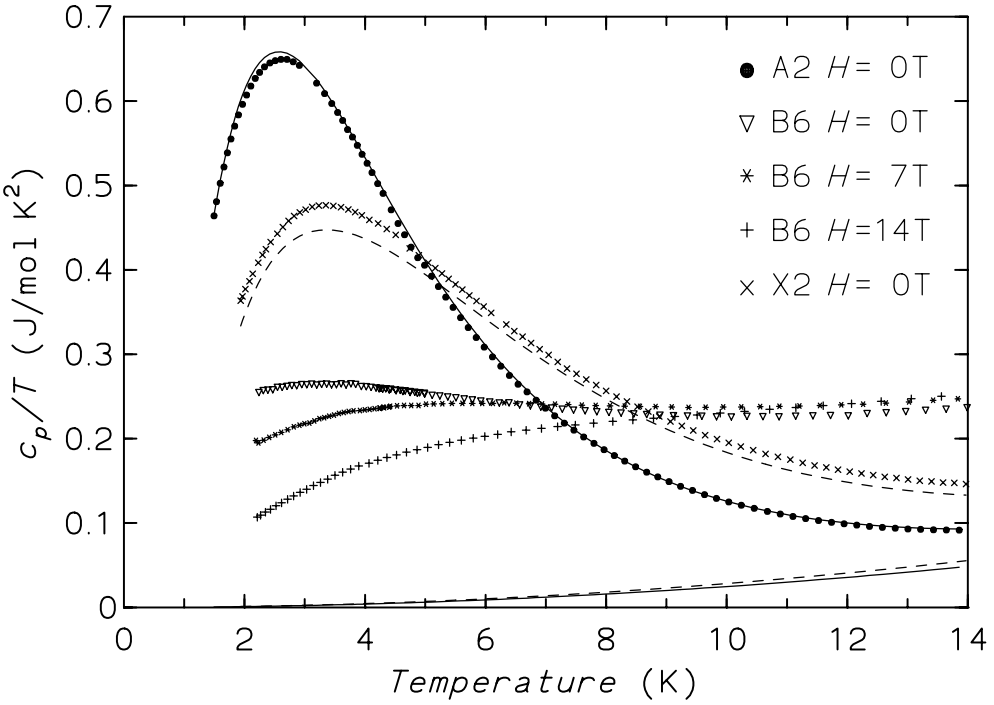

Figure 8. Low-temperature specific heat capacities $c_p(T, B_{\text{ext}})$ of samples A2 and X2 in 0 T and of sample B6 in 0 T, 7 T, and 14 T magnetic fields. The continuous (A2) and the dashed (X2) curves show fits and their lattice contributions (see the text).

The low-T specific heat of sample B6 in zero field (figure 8) is nearly linear in T. It can be described by a huge quasi-linear term $\gamma^* T$ of 240 ± 15 mJ mol^{-1} K^{-2} plus a small maximum around 3.5 K plus a lattice contribution. Obviously the energy splitting of the Nd^{3+} ground state is much larger in this oxygen-reduced sample than in samples A2 and X2, and the related entropy is shifted to higher T. It is also clear from figures 5 and 7 that a large part of the magnetic entropy from the ordering of the Mn sublattice is shifted to lower T in comparison to the case for sample A2 with $\delta \approx 0$. Thus the overlap of the two magnetic contributions is responsible for the quasi-linear behaviour of $c_p(T)$ below 20 K. There is a very broad distribution of the level splitting of Nd^{3+} in sample B6. Also the median energy splitting of this distribution is larger than for samples A2 and X2. The wide distribution can be explained by a strong disorder on the B site or a large variation in Mn–O–Mn magnetic exchange strength. The larger average value of the molecular field seems to be in contrast to the reduced magnetization of sample B6 with respect to sample A2. The increase in molecular field at the perovskite A site has to be related to strong afm interactions. The remaining spontaneous moment below 120 K has to be assigned to a spin canting on the predominantly afm-ordered Mn sublattice. A change of the g-factor of the Nd^{3+} ground state with δ seems unlikely.

A comparison with the corresponding $Nd_{0.67}Sr_{0.33}MnO_3$ sample of Gordon *et al* [34] shows that our sample A2 (and also sample X2) is of superior quality. A2 contains no Mn_3O_4 impurity, and for X2 the Mn_3O_4 anomaly in $c_p(T)$ is smaller than for the sample in [34]. Also the c_p-peak signalling the Mn-sublattice ordering occurs only at 205 K and is quite broad (figure 1 in [34]) compared to that for our sample A2. The observation of a large 'T-dependent

"linear term", $\gamma(T)T$' in [34] seems to have a similar explanation as that for our sample B6, namely a significant oxygen deficiency δ. However, we agree with Gordon *et al* that the linear term is of magnetic origin. Pure $Nd_{0.67}Sr_{0.33}MnO_{3-\delta}$ with $\delta \simeq 0$ has an electronic linear term of the same size as found for the La manganites [31, 32].

External magnetic fields applied to sample B6 lead to a further shift of Nd^{3+}-derived entropy to higher T, i.e. the Mn-sublattice molecular field and external field sum. From a comparison of the zero-field and the 14 T data, the molecular field can be estimated to be of the same magnitude, in agreement with [34].

5. Conclusions

Measurements of resistivity, susceptibility, and heat capacity for $Nd_{0.67}Sr_{0.33}MnO_{3-\delta}$ samples subjected to various annealing conditions lead to the following results and conclusions. For a fixed cationic composition of $Nd_{0.67}Sr_{0.33}MnO_{3-\delta}$ in well annealed and highly oxidized samples, only a sharp anomaly occurs at the Mn-sublattice pm–fm transition at $T_C = 246$ K in the resistivity, magnetization, and specific heat. With decreasing P_{O_2} and thus increasing oxygen deficiency δ, the Mn^{4+}/Mn^{3+} ratio decreases. $\rho(300\ \mathrm{K})$ increases strongly and a second broad anomaly develops in $\rho(T)$ and masks the magnetic transition in $\rho(T)$ completely. The pm–fm transition is readily seen in the heat capacity, and remains nearly the same for all samples annealed under $P_{O_2} > 6.3 \times 10^{-2}$ Pa. The changes in the magnetization and of the weight of the sample in a TGA prove that oxygen is taken out of the bulk of the samples. Changes in $\rho(T)$, even for the smallest δ, might also be due to the degradation of grain boundaries.

In a sample reduced in an Ar/5% H_2 atmosphere, the Mn-sublattice magnetic ordering temperature is reduced to $\approx$120 K. While samples with $\delta \approx 0$ display a broadened Schottky-like anomaly in $c_p(T)$ below 20 K (from a Mn-molecular-field-split Nd^{3+} ground-state doublet), this anomaly is absent in the Ar/5% H_2-reduced sample. It is shown that a huge quasi-linear term in $c_p(T)$ for the latter sample is a combination of magnetic contributions of both the Mn and Nd sublattices. Thermodynamic standard data (enthalpy, entropy) at 298.15 K have been determined.

The study demonstrates the strong influence of oxygen deficiency δ (i.e. the annealing conditions) on magnetic and transport properties of mixed-valence RE manganites, emphasizes the requirement of controlling the sample preparative conditions carefully, and shows how drastically the detailed defect chemistry and disorder on the perovskite B site can influence low-temperature magnetic and transport properties in manganites.

Acknowledgments

A Poddar and P Murugaraj gratefully acknowledge fellowships granted by the Alexander von Humboldt foundation and the Max-Planck-Gesellschaft, respectively. We thank E Brücher, N Rollbühler, G Siegle and R W Henn for susceptibility and resistivity measurements and x-ray diffraction, E Schmitt for DSC measurements, and L Viczian and O Buresch for chemical analyses. We wish to thank K Bärner for discussions.

References

[1] Jonker G H and van Santen J H 1950 *Physica* **16** 337
[2] Goodenough J B and Longo J M 1970 *Landolt–Börnstein New Series* Group III, vol 4a, ed K H Hellwege (Berlin: Springer)
[3] von Helmolt R, Wecker J, Holzapfel B, Schultz L and Samwer K 1993 *Phys. Rev. Lett.* **71** 2331

[4] Goodenough J B 1997 *J. Appl. Phys.* **81** 5330
[5] Tokura Y 1997 *Physica* B **237–238** 1
[6] Rao C N R, Mahesh R, Raychaudhuri A K and Mahendiran R 1998 *J. Phys. Chem. Solids* **59** 487
[7] Steele B C H 1997 *Solid-State Ion.* **94** 239
[8] Zener C 1951 *Phys. Rev.* **82** 403
[9] Anderson P W and Hasegawa H 1955 *Phys. Rev.* **100** 675
[10] de Gennes P G 1960 *Phys. Rev.* **118** 141
[11] Imada M, Fujimori A and Tokura Y 1998 *Rev. Mod. Phys.* **70** 1039
[12] Kuwahara H, Tomioka Y, Asamitsu A, Moritomo Y and Tokura Y 1995 *Science* **270** 961
Tomioka Y, Asamitsu A, Kuwahara H, Moritomo Y, Kasai M, Kumai R and Tokura Y 1997 *Physica* B **237–238** 6
[13] Arulraj A, Santhosh P N, Gopalan R S, Guha A, Raychaudhuri A K, Kumar N and Rao C N R 1998 *J. Phys.: Condens. Matter* **10** 8497
[14] Ramirez A P, Schiffer P, Cheong S-W, Chen C H, Bao W, Palstra T T M, Gammel P L, Bishop D J and Zegarski B 1996 *Phys. Rev. Lett.* **76** 3188
Ramirez A P, Cheong S-W and Schiffer P 1997 *J. Appl. Phys.* **81** 5337
Ramirez A P 1997 *J. Phys.: Condens. Matter* **9** 8171
[15] Garfield N J, Howson M A and Paul D M^{c}K 1996 *Czech. J. Phys. Suppl.* S3 **46** 1225
[16] Millis A J, Littlewood P B and Shraiman B I 1995 *Phys. Rev. Lett.* **74** 5144
[17] Xiong G C, Li Q, Ju H L, Greene R L and Venkatesan T 1995 *Appl. Phys. Lett.* **66** 1689
[18] Tanaka J, Umehara M, Tamura S, Tsukioka M and Ehara S 1982 *J. Phys. Soc. Japan* **51** 1236
[19] Satyalakshmi K M, Fisher B, Patlagan L, Koren G, Sheriff E, Prozorov R and Yeshurun Y 1998 *Appl. Phys. Lett.* **73** 402
[20] Neumeier J J, Andres K and McClellan K J 1999 *Phys. Rev.* B **59** 1701
[21] Hueso L E, Rivadulla F, Sánchez R D, Jardón C, Vázquez-Vázquez C, Rivas J and López-Quintela M A 1998 *J. Magn. Magn. Mater.* **189** 321
[22] Gupta A, Gong G Q, Xiao G, Duncombe P R, Lecoeur P, Trouilloud P, Wang Y Y, Dravid V P and Sun J Z 1996 *Phys. Rev.* B **54** 15 629
[23] Jin S, Tiefel T H, McCormack M and Bryan H M O 1995 *Appl. Phys. Lett.* **67** 557
[24] De Léon-Guevara A M, Berthet P, Berthon J, Millot F, Revcolevschi A, Anane A, Dupas C, Le Dang K, Renard J P and Veillet P 1997 *Phys. Rev.* B **56** 6031
[25] Ghivelder L, Abrego Castillo I, Gusmaõ M A, Alonso J A and Cohen L F 1999 *Phys. Rev.* B **60** 12 184
[26] Ju H L, Kwok C, Li Q, Greene R L and Venkatesan T 1994 *Appl. Phys. Lett.* **65** 2108
[27] Ju H L and Sohn H 1997 *J. Magn. Magn. Mater.* **167** 200
[28] Ju H L, Gopalakrishnan J, Peng J L, Li Q, Chiong G C, Venkatesan T and Greene R L 1995 *Phys. Rev.* B **51** 6143
[29] Medvedeva I V, Bersenev Yu S, Bärner K, Haupt L, Mandal P and Poddar A 1997 *Physica* B **229** 194
[30] Babushkina N A, Belova L M, Ozhogin V I, Gorbenko O Yu, Kaul A R, Bosak A A, Khomskii D I and Kugel K I 1998 *J. Appl. Phys.* **83** 7369
Ibarra M R, Zhao G-M, Arnold Z, Marquina C, Algarabel P A, Keller H and Ritter C 1998 *Phys. Rev.* B **57** 7446
Zhou J-S and Goodenough J B 1998 *Phys. Rev. Lett.* **80** 2665
[31] Coey J M D, Viret M, Ranno L and Ounadjela K 1995 *Phys. Rev. Lett.* **75** 3910
[32] Woodfield B F, Wilson M L and Byers J M 1997 *Phys. Rev. Lett.* **78** 3201
[33] Ghivelder L, Abrego Castillo I, Alford N McN, Tomka G J, Rieldi P C, MacManus-Driscoll J, Akther Hossain A K M and Cohen L F 1998 *J. Magn. Magn. Mater.* **189** 274
[34] Gordon J E, Fisher R A, Jia Y X, Phillips N E, Reklis S F, Wright D A and Zettl A 1998 *J. Magn. Magn. Mater.* **177–181** 856
Gordon J E, Fisher R A, Jia Y X, Phillips N E, Reklis S F, Wright D A and Zettl A 1999 *Phys. Rev.* B **59** 127
[35] Fernández-Díaz M T, Martínez J L, Alonso J M and Herrero E 1999 *Phys. Rev.* B **59** 1277
[36] Sasaki K and Maier J 1999 *J. Appl. Phys.* **86** 5422
[37] Henggeler W, Roessli B, Furrer A, Vorderwisch P and Chatterji T 1998 *Phys. Rev. Lett.* **80** 1300
Zwicknagl G and Fulde P 1999 *Phys. Rev. Lett.* **82** 2217
Henggeler W, Roessli B, Furrer A, Vorderwisch P and Chatterji T 1999 *Phys. Rev. Lett.* **82** 2218
[38] Uma S, Schnelle W, Gmelin E, Rangarajan G, Skanthakumar S, Lynn J W, Walter R, Lorenz T, Büchner B, Walker E and Erb A 1998 *J. Phys.: Condens. Matter* **10** L33
[39] Gmelin E 1987 *Thermochim. Acta* **110** 183
[40] Kröger F A and Vink J J 1956 *Solid State Physics* vol 3, ed H Ehrenreich, D Turnbull and F Seitz (New York: Academic) p 307
[41] Dominguez M, Bhagat S M, Lofland S E, Ramachandran J S, Xiong G C, Hu H C, Venkatesan T and Greene R L 1995 *Europhys. Lett.* **32** 349

[42] Worledge D C, Snyder G J, Hiskes R, DiCarolis S, Beasley M R and Geballe T H 1996 *J. Appl. Phys.* **80** 5158
[43] Itoh M, Nishi K, Yu J D and Inaguma Y 1997 *Phys. Rev.* B **55** 14 408
[44] Tanaka J and Mitsuhashi T 1984 *J. Phys. Soc. Japan* **53** 24
[45] Bärner K and Gmelin E 1985 *Phys. Status Solidi* b **132** 431
[46] Park S H, Jeong Y H, Lee K B and Kwon S J 1997 *Phys. Rev.* B **56** 67
[47] Podlesnyak A, Rosenkranz S, Fauth F, Marti W, Furrer A, Mirmelstein A and Scheel H J 1993 *J. Phys.: Condens. Matter* **5** 8973
[48] Goodman G L, Loong C-K and Soderholm L 1991 *J. Phys.: Condens. Matter* **3** 49
[49] Raju N P, Gmelin E and Kremer R K 1992 *Phys. Rev.* B **46** 5405